EPR study of Fe^{3+} in α-quartz: Characterization of a new type of cation-compensated center

J. Minge,* J. A. Weil, and D. G. McGavin†
Department of Chemistry, University of Saskatchewan, Saskatoon, Saskatchewan, Canada S7N 0W0
(Received 26 June 1989)

A new type of cation-compensated Fe^{3+} ($S=\frac{5}{2}$) center designated $[FeO_4/M]^0_\beta$, with $M=$Li and H, has been found to exist in synthetic iron-doped α-quartz, through an X-band electron paramagnetic resonance study. The spin-Hamiltonian parameters at temperature approximately 20 K were determined for both centers, allowing for anisotropy of the g factor as well as **g**- and **D**-matrix noncoaxiality, and including high-spin terms of the form S^4. While the ^{7}Li hyperfine matrix was not obtainable, the EPR measurements did yield the proton hyperfine matrix for $M=$H. For $M=$Li, in contrast to the C_2 symmetry of the previously studied $[FeO_4/Li]^0_\alpha$, center β shows C_1 symmetry at low temperatures (20 K), but approaches C_2 symmetry at higher temperatures (approximately ≥ 160 K). The hydrogenic center, designated as $[FeO_4/H]^0_\beta$, shows C_1 symmetry up to room temperature. The analysis of the spin-Hamiltonian parameter matrices for both the α (the previously studied form) and the β form of the cation-compensated Fe^{3+} centers indicates that the (interstitial) M ion is located, respectively, at opposite sides of the slightly distorted [Si(Fe)O_4] "tetrahedron."

I. INTRODUCTION

In α-quartz, many of the substitutional (for Si) impurity 3+ ions such as Al, Ge, Ti, and Fe are known to be associated each with a nearby interstitial proton or +1 alkali-metal ion which provides electric charge compensation for the whole defect.[1] The $[SiO_4]^0$ unit in pure α-quartz forms a slightly distorted "tetrahedron," with the central Si atom positioned on a crystal twofold polar symmetry axis; here two pairs $O(1,2)_<$ and $O(3,4)_>$ of equivalent oxygen atoms respectively form "shorter" and "longer" bonds with the Si atom. The question of how many different forms (configurations) of a given center can actually exist in α-quartz and how their structural details affect the center's relative stability and possible interconversion among the configurations is of considerable interest. Consistent with the low local symmetry (C_1 or at most C_2) in α-quartz, a variety of structurally and energetically different configurations of a given center associated with a specific compensating ion can occur. For those substitutional centers which exhibit the C_2 symmetry, the substitutional ion as well as the compensating ion is located (at least on a time average) on the twofold axis. The possible position of the latter ion on the axis at either side of the "tetrahedron" should result, in principle, in existence of (at least) two distinct forms of the center. Considering here only paramagnetic centers, we note that indeed two forms of Ge^{3+} and Ti^{3+} centers (i.e., $[GeO_4/M]^0_{A,C}$ (Ref. 2) and $[TiO_4/M]^0_{A,B}$ (Refs. 3–5)) are known to exist in α-quartz; however, to date, only one form of $[AlO_4/M]^+$ (Ref. 6) has been reported.

Recently, in our series of detailed electronic paramagnetic resonance (EPR) and electron-nuclear double resonance (ENDOR) studies of the various Fe^{3+} centers in crystalline α-quartz, we have reexamined the center now labeled $[FeO_4/Li]^0_\alpha$ (Ref. 7) and find that it shows C_2 symmetry down to 4 K. Herein, we now report the discovery of a second type of such a center, denoted by $[FeO_4/Li]^0_\beta$, which shows C_1 symmetry at low temperatures (ca. 20 K). However, as the temperature is raised, $[FeO_4/Li]^0_\beta$ approaches C_2 symmetry. This occurs at temperatures above 160 K. Such a thermally activated transition was recently observed for center $[FeO_4/Na]^0$ in α-quartz,[8,9] and some tentative models involving an Na^+ ion hopping across a twofold crystal symmetry axis were considered.[9] Herein, we also present the details of EPR spectral analysis of a newly discovered hydrogen-compensated Fe^{3+} (labeled β type) center, which also occurs in α-quartz along with the recently characterized $[FeO_4/H]^0_\alpha$ center.[10]

It is now becoming clear that the electrically compensated Fe^{3+} centers (where Fe^{3+} substitutes for Si^{4+}) can exist in two forms α and β differing mainly in the location of the compensating ion, which can be positioned at either side of the slightly distorted [Si(Fe)O_4] "tetrahedron." The preceding dichotomy has yet to be proven in the case of the Na-compensated Fe^{3+} center, for which only one form is known so far.

The substantial differences between the H^+-, Li^+-, and Na^+-compensated trivalent iron centers,[10,11] and especially the thermally induced symmetry transition effects ($C_1 \leftrightarrow C_2$) shown by some of them,[8,9] are not explainable solely by the location(s) of the compensating ion.

II. EXPERIMENTAL

The same (lithium-containing) iron-doped (ca. 50 ppm) and (partially) hydrogen-electrodiffused crystalline quartz sample as used in the previous study, of center $[FeO_4/H]^0_\alpha$,[10] was used in the present investigation. In our search for other forms of lithium- and hydrogen-

compensated Fe^{3+} centers in α-quartz, the crystal was first annealed for ca. 20 h at temperatures of ca. 450 °C and then x irradiated for 1 h at temperature 77 K. The cold crystal was then quickly transferred and mounted in the EPR cavity where it was cooled to ca. 20 K. The most intense EPR lines observed after that treatment were still those stemming from the previously studied $[FeO_4/Li]^0_\alpha$, $[FeO_4/H]^0_\alpha$, and $[AlO_4]^0$ (Ref. 12) centers (which served to permit alignment of the crystal with accuracy $\pm 2'$ of arc). Second in intensity were lines originating from the two new centers $[FeO_4/Li]^0_\beta$ and $[FeO_4/H]^0_\beta$. The relative intensity ratio between the β and α forms was ca. 0.04 for the former and ca. 0.009 for the latter center (the measurements were done with $\hat{\mathbf{B}}\|\hat{\mathbf{c}}$ using the fine-structure EPR line 3-4, i.e., the transitions between states labeled with $m_s = -\frac{1}{2}$ and $\frac{1}{2}$ in the high-field-limit scheme; see Fig. 1). Further inspection revealed the presence also of weak lines belonging to the four-hydrogen and three-hydrogen,[13] and $[AlO_4]^+$ (Ref. 14) centers, as well as some lines of yet unknown centers. Not even traces of $[FeO_4]^-$ (Ref. 15) or of $[FeO_4/Na]^0$ (Ref. 16) centers were detected. A comparison of c-axis EPR spectra (i.e., $\hat{\mathbf{B}}\|\hat{\mathbf{c}}$) of this sample (and also of a sodium-electrodiffused crystal not subjected to x-irradiation) before and after the above-described treatment revealed that both newly discovered $[FeO_4/Li]^0_\beta$ and $[FeO_4/H]^0_\beta$ centers had in fact already been present in unirradiated crystals. It appears that while x irradiation increased the β/α concentration ratio of the hydrogen-compensated Fe^{3+} centers by a factor of ca. 2.5, this treatment resulted in a decrease of this ratio of the lithium-compensated Fe^{3+} centers by more then 2.7 times. Increase of temperature acts in just the opposite way. It was observed, when the crystal was warmed to room temperature over a two-day period and then recooled to ca. 20 K that the ratio β/α increased to ca. 0.06 for the Li-compensated centers but decreased to ca. 0.007 for the H-compensated centers. No additional absorptions, due to centers containing ^{57}Fe (Ref. 17) or neighbor ^{29}Si could be detected, since the primary β-center spectra were relatively weak.

Following the report by Choi and Choh,[18] we found not only the two centers reported by them but also a third such center. All three are similar to $[FeO_4/Li]^0_\alpha$. At a temperature of ca. 20 K their abundance was approximately 1.3%, 0.6%, and 0.4%, respectively, of that of $[FeO_4/Li]^0_\alpha$, which is 1–2 orders of magnitude less than reported in Ref. 18. No attempt was made to study these centers in any detail.

In our work, to describe any general orientation of the external magnetic field vector $\hat{\mathbf{B}}$ relative to the $\hat{\mathbf{c}}$ (the crystal threefold screw symmetry axis) and to the axes $\hat{\mathbf{a}}_i$ (crystal twofold symmetry axes $\perp\hat{\mathbf{c}}$, $i = 1,2,3$), polar angle θ and azimuthal angle φ are used, where $\theta = \sphericalangle(\hat{\mathbf{c}},\hat{\mathbf{B}})$ and $\varphi = \sphericalangle(\hat{\mathbf{a}}_1,\hat{\mathbf{c}}\otimes\hat{\mathbf{B}}\otimes\hat{\mathbf{c}})$.

The sample was mounted in the EPR cavity such that $\hat{\mathbf{a}}_1\perp\hat{\mathbf{B}}$ and $\hat{\mathbf{a}}_1\|\hat{\mathbf{B}}_1$ (linearly polarized cw microwave magnetic field). An EPR line-position data set was collected at ca. 20 K using a low-temperature EPR cavity system[19] and a Varian V4502 spectrometer operated at a fixed fre-

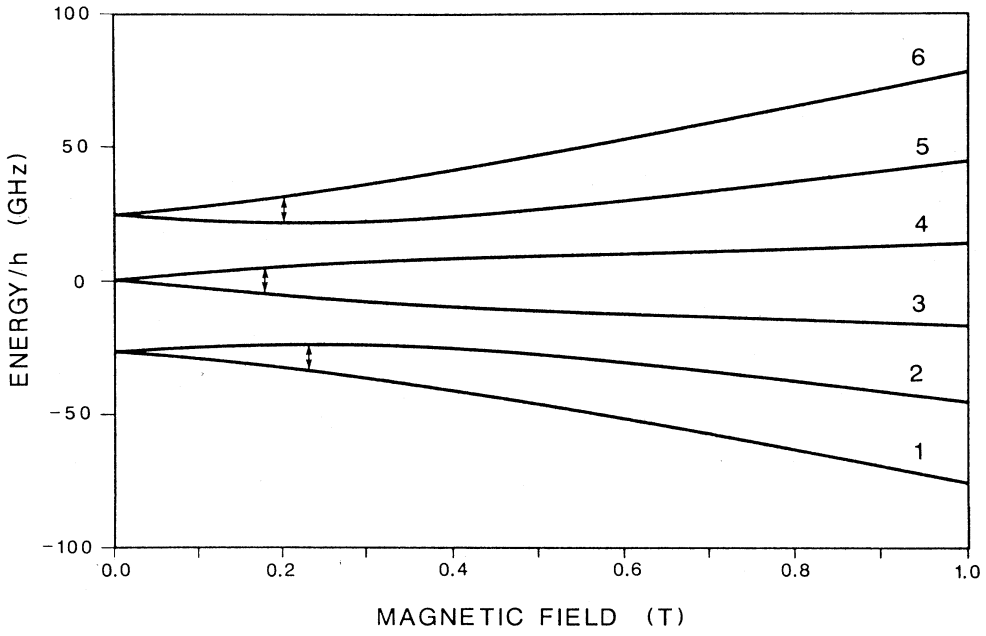

FIG. 1. The energy levels for $[FeO_4/Li]^0_\beta$ as a function of external magnetic field B ($\hat{\mathbf{B}}\|\hat{\mathbf{c}}$). The levels corresponding to the high-field m_s quantum numbers $-\frac{5}{2}$, $-\frac{3}{2}$, $-\frac{1}{2}$, $\frac{1}{2}$, $\frac{3}{2}$, and $\frac{5}{2}$ are numbered in order (increasing energy) from 1 to 6. No hyperfine splittings are included. Transitions at 9.915 GHz are indicated, and occur at (calculated) fields 175.94, 198.80, and 227.30 mT.

quency of ca. 9.93 GHz. Rotation angles were measured with a precision of $\pm 1'$ of arc. Our microwave-frequency values and line-position field data have estimated uncertainties of 1×10^{-6} GHz and 1×10^{-3} mT, respectively. The magnetic field B was measured using a proton NMR gaussmeter and then corrected slightly to take into account the difference in position between the NMR probe and the quartz sample (see Ref. 7).

The experimentally observed EPR transitions were numerically processed using a recently updated computer program[15] involving exact diagonalization of the whole spin-Hamiltonian matrix and iterative least-squares fitting.

For the $[FeO_4/Li]^0_\beta$ center, rotation data were collected in 10° steps for the 3-4 fine-structure lines, over a 180° range in the plane $\hat{\mathbf{B}}\perp\hat{\mathbf{a}}_1$, and at 1° intervals around the extrema of the other fine-structure line positions. In the rotation plane already defined, three doubly degenerate EPR absorptions from the center $[FeO_4/Li]^0_\beta$ are observed (at temperature ca. 20 K) for each of the fine-structure transitions (see Fig. 2), thus revealing the C_1 local symmetry at the center.[20] These degenerate EPR lines [labeled (1,1'), (2,3'), and (3,2')] originate from six respective sites (configurations) of the center $[FeO_4/Li]^0_\beta$ in the α-quartz structure, where sites i and i' ($i=1,2,3$) are related by operation of twofold crystal symmetry axis $\hat{\mathbf{a}}_i$. As the temperature is increased, lines (2,3') and (3,2') approach each other and then coalesce near 160 K (at X band). Besides, all lines [including type (1,1')] tend to broaden, and are hardly observable at room temperature.

At only a few orientations, the fine-structure EPR lines of $[FeO_4/Li]^0_\beta$ show resolved hyperfine structure, resulting very probably from interaction of the unpaired electrons of the Fe^{3+} ion with the nuclear magnetic moment of the nearby lithium(7) ion ($I=\frac{3}{2}$, 92.5% abundance). However, no attempts were made to derive the ^{7}Li hyperfine matrix from the generally poorly resolved EPR hyperfine spectra; here, ENDOR studies will be required. The observed hyperfine patterns (e.g., Fig. 3) as well as the hyperfine splitting of ca. 0.12 mT resemble those observed for the center $[FeO_4/Li]^0_\alpha$ studied previously.[7] The fact that a five-component hyperfine spectrum can be observed [Fig. 3(b)] proves that we are dealing with a nuclear spin $I>\frac{1}{2}$; this eliminates the H^+ ion as a possible source of the splitting. There is strong evidence that no Na^+ ions are present in our sample, i.e., no EPR absorption from $[FeO_4/Na]^0$ was observed. Thus our choice of Li^+ ion as a compensator seems to be reasonable. Additional evidence for this comes from comparison of the spin-Hamiltonian parameter matrices of the center studied here with those of $[FeO_4/Li]^0_\alpha$ (see the discussion below).

The spin Hamiltonian used for $[FeO_4/Li]^0_\beta$ is similar to the one utilized by Mombourquette *et al.*[10] for $[FeO_4/H]^0_\alpha$ except that now no nuclear terms are included. Since the center $[FeO_4/Li]^0_\beta$ has C_1 symmetry, no constraints on any spin-Hamiltonian parameters were imposed.

For the $[FeO_4/H]^0_\beta$ center, it is worth mentioning that, as in the case of $[FeO_4/H]^0_\alpha$, the single-proton hyperfine structure varies greatly with field B, fine-structure transition and crystal orientation. Thus two-, three- (see Fig. 4), or four-component structure can be observed (at least below 0.3 T). The absorption first-derivative linewidths vary from ca. 0.05 mT for an individual hyperfine line in the lowest-field region to 0.75 mT for the lines (not showing resolved hyperfine structure) in the 1 T region, and even greater widths occur at orientations at which the slope of the line position versus angle (for rotation about $\hat{\mathbf{a}}_1$) is steepest. The linewidth effect may be caused by D strain, i.e., variation in **D**-matrix parameters with location in the crystal.

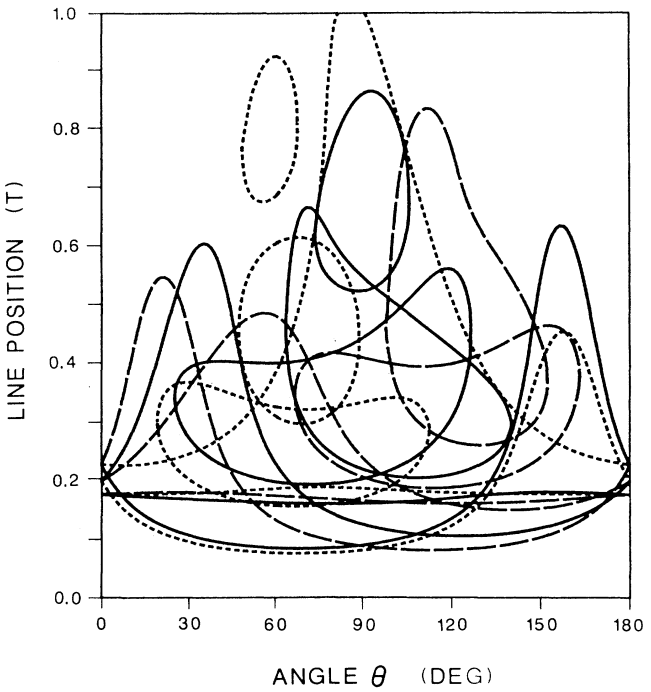

FIG. 2. Calculated EPR line positions (data from Table I) for $[FeO_4/Li]^0_\beta$ at 9.915 GHz and $T=20$ K as a function of crystal rotation about its twofold axis $\hat{\mathbf{a}}_1$. All symmetry-related sites are included. Solid curves: sites 1,1'; dashed curves: sites 2,3'; dotted curves: sites 3,2'. The ^{7}Li hyperfine structure is not discernible on the field scale used. Angle 0° is at $\hat{\mathbf{B}}\|\hat{\mathbf{c}}$, and 90° is at $\hat{\mathbf{B}}\|\hat{\mathbf{Y}}$ ($\perp\hat{\mathbf{a}}_1$ and $\hat{\mathbf{c}}$).

To determine the required spin-Hamiltonian parameters, all experimentally accessible (intense enough) EPR transitions of $[FeO_4/H]^0_\beta$ in the rotation plane ($\hat{\mathbf{B}}\perp\hat{\mathbf{a}}_1$) were explored (Fig. 5). Basically the data (i.e., resonance magnetic field at actual experimental frequency and crystal orientation) were taken in 10° steps, but 1° intervals were used near the turning points. The same spin Hamiltonian as was used for $[FeO_4/H]^0_\alpha$ (see Ref. 10) was utilized here, since both centers have the same symmetry.

III. RESULTS AND DISCUSSION

A. $[FeO_4/Li]^0_\beta$

We have accurately determined the spin-Hamiltonian parameters[15] including matrices **g**, **D**, and the Stevens pa-

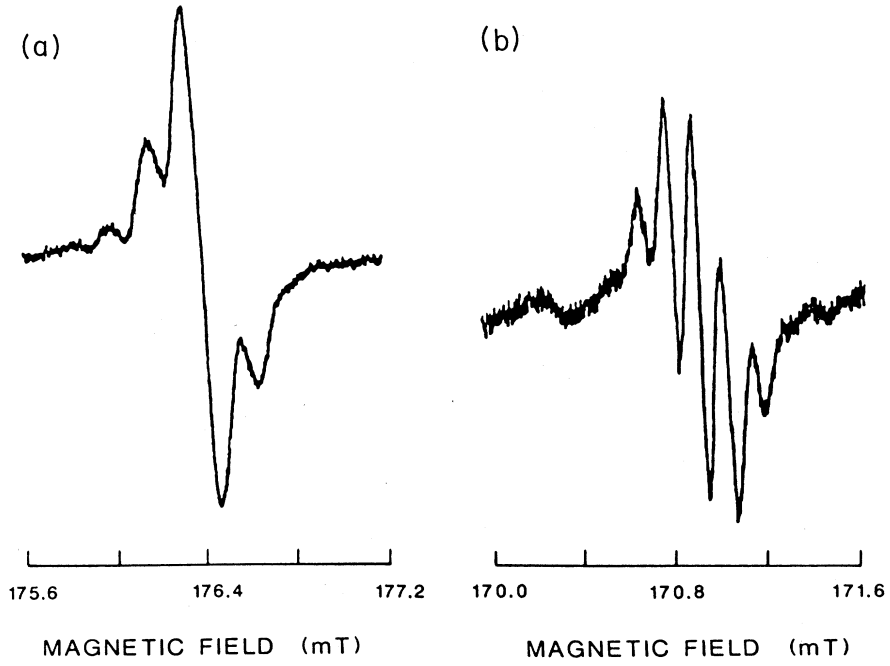

FIG. 3. Part of the first-derivative 20 K EPR spectrum of $[FeO_4/Li]^0_\beta$ (site 1) at 9.9353 GHz, showing the ^{7}Li hyperfine lines of the 3–4 (m_s: $-\frac{1}{2}$ to $\frac{1}{2}$) transition observed respectively at crystal orientations: (a) $\theta=0°$, $\varphi=90°$. (b) $\theta=20°$, $\varphi=90°$. The small peak visible in the low-field region is, in both cases, due to an extraneous center.

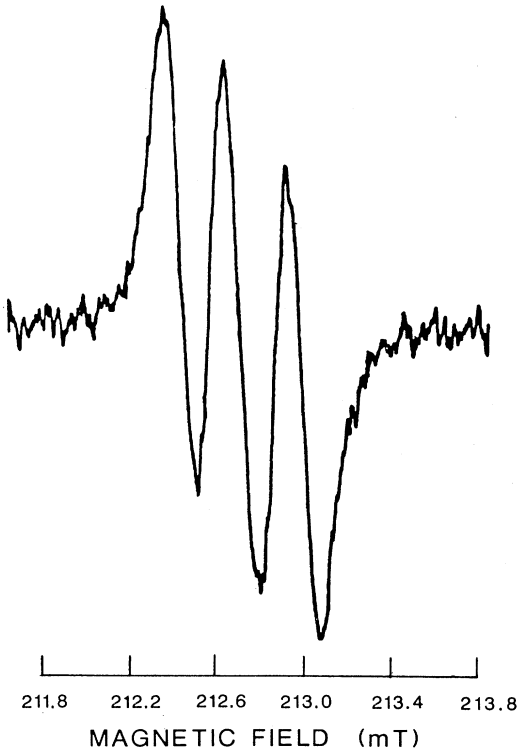

FIG. 4. First-derivative EPR spectrum for $[FeO_4/H]^0_\beta$ at 9.938 58 GHz, showing the ^{1}H hyperfine lines of the 3↔4 (high-field quantum numbers m_s: $-\frac{1}{2}\leftrightarrow\frac{1}{2}$) transition, taken with $\hat{\mathbf{B}}\|\hat{\mathbf{c}}$ at ca. 20 K. Simulation of a similar three-line hyperfine spectrum arising from presence of a single proton can be seen in Fig. 2 of Ref. 10.

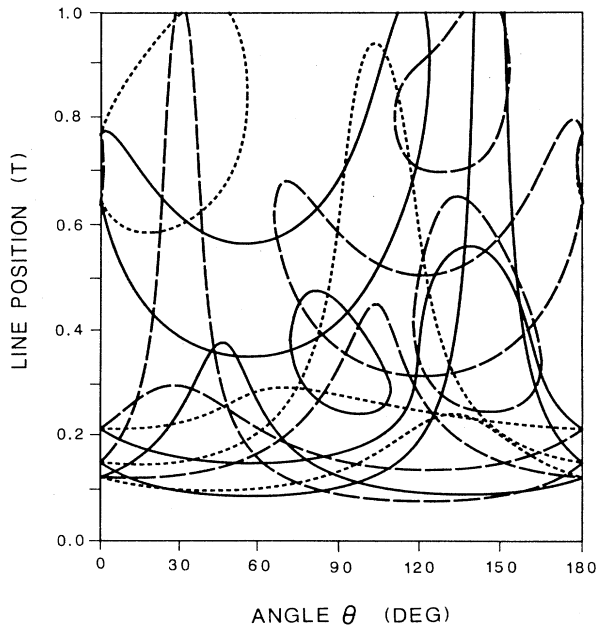

FIG. 5. Calculated EPR line positions (data from Table III) for $[FeO_4/H]^0_\beta$ at 9.915 GHz and $T=20$ K as a function of crystal rotation about twofold axis $\hat{\mathbf{a}}_1$. All symmetry-related sites are included, giving three doubly degenerate lines for each transition. Solid curves: site 1 (and 1′); dashed curves: site 2 (and 3′); dash-dotted curves: site 3 (and 2′). The ^{1}H hyperfine structure is not included. Angle 0° is at $\hat{\mathbf{B}}\|\hat{\mathbf{c}}$, and 90° is at $\hat{\mathbf{B}}\|\hat{\mathbf{y}}$ ($\perp\hat{\mathbf{a}}_1$ and $\hat{\mathbf{c}}$). The lines for all six symmetry-related $[FeO_4/H]^0_\beta$ sites superimpose at 0°.

TABLE I. $[FeO_4/Li]^0_\beta$ principal values and directions of matrices $\mathbf{Y}=\mathbf{g}$ and $\mathbf{D}$ in the crystal Cartesian coordinate system[a] for site 1 at ca. 20 K, derived from the EPR data. The S^4 parameters B_4^m are given (Ref. 15). The estimated uncertainties in the last significant figures are included, in parentheses.

	Y		k	Y_k	θ_k	φ_k	
			g				
2.004 53(16)	−0.001 10(17)		0.000 17(12)	1	2.005 37(16)	81.0(3.8)	323.8(2.4)
	2.003 84(14)		−0.000 11(9)	2	2.004 04(14)	9.1(4.9)	139.0(32.6)
			2.004 07(12)	3	2.003 03(20)	90.7(5.8)	53.7(2.6)
			D/h (MHz)				
−1193.3(6)	−3983.8(5)		286.8(4)	1	5022.3(6)	70.751(4)	121.880(2)
	1559.8(6)		2394.4(6)	2	−328.3(5)	30.042(6)	354.738(10)
			−366.5(5)	3	−4693.9(7)	112.133(7)	40.046(4)
			B_4^m/h (MHz)				
B_4^0/h	0.183(70)						
B_4^1/h	0.591(114)	B_4^2/h	4.131(51)	B_4^3/h	−1.187(173)	B_4^4/h	− 2.398(64)
B_4^{-1}/h	1.078(92)	B_4^{-2}/h	−0.672(25)	B_4^{-3}/h	−1.898(194)	B_4^{-4}/h	−1.070(65)

[a]Ref. 15, Table II: coordinate system (1); note that any principal direction defined by angles θ_k and φ_k equivalently can be described by angles $\theta'_k=180°-\theta_k$ and $\varphi'_k=180°+\varphi_k$.

rameters B_4^m for S^4 terms (Table I). These parameters were obtained from averaged EPR line positions (each taken as the center of gravity of the lithium hyperfine pattern, if observed). No attempts were made to fit our data with higher-order Zeeman terms of the type BS^3 and BS^5. The final RMS deviation between the 115 observed and calculated EPR line positions was 0.056 mT. Only the relative signs of the S^2 (**D** matrix) and S^4 parameters were determined, i.e., the absolute signs of the whole **D** and S^4 parameter array remain undetermined (compare Refs. 7 and 10). In Table I, the set of spin-Hamiltonian parameters was chosen with signs such that the **D** matrix matches (closely, in fact) the one reported[7] for $[FeO_4/Li]^0_\alpha$.

The sets of all possible EPR line positions ($\hat{\mathbf{B}}\perp\hat{\mathbf{a}}_1$) within the magnetic field range 0–1 T, for fixed microwave frequency 9915 MHz, are shown in Fig. 2. Figure 1 shows an energy-level diagram as a function of magnetic field B, for $\hat{\mathbf{B}}\|\hat{\mathbf{c}}$, with the observed EPR transitions indicated. A corresponding simulated c-axis spectrum is presented in Fig. 6, and agrees very well with the observed one.

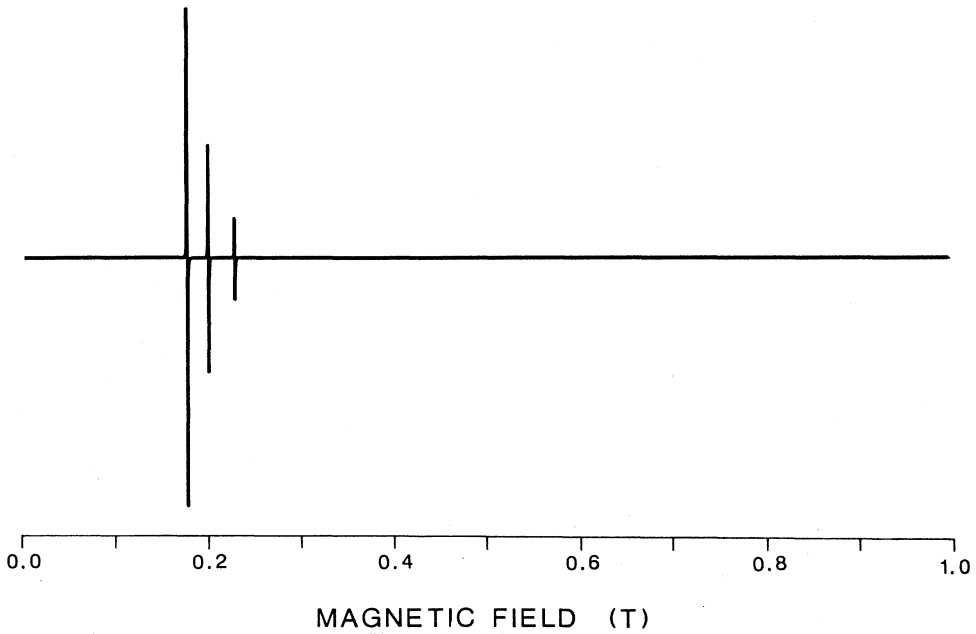

FIG. 6. First-derivative EPR spectrum for $[FeO_4/Li]^0_\beta$ at 9.915 GHz simulated from the best-fit 20 K spin-Hamiltonian parameters in Table I, for $\hat{\mathbf{B}}\|\hat{\mathbf{c}}$ and excitation field $\hat{\mathbf{B}}_1\|\hat{\mathbf{a}}_1$. The same transitions as depicted in Fig. 1 are shown. The ^{7}Li hyperfine splitting is not visible at the field scale used. The spectrum agrees well with the observed one.

The **g** matrix for the center $[FeO_4/Li]^0_\beta$ studied here is not uniaxial (Table I), as is also found for the hydrogen-compensated Fe^{3+} centers in α-quartz.[10] Its principal values do not differ much from those of the corresponding α-type center (e.g., the smallest g value is still close to the free-electron value). We note that the principal axes of **g** do not match any of the Si-O directions (see Ref. 15, Table V) of the pure quartz $[SiO_4]^0$ unit (the smallest difference in angle between one of them and the closest Si—O bond is 23.9°). It seems significant that in the β-type center the direction corresponding to the largest principal value of the **D** matrix is close (7.7°) to the direction of the Si—O(2) bond. This suggests (compare situation in centers $[FeO_4/H]^0_{\alpha,\beta}$) that in $[FeO_4/Li]^0_\beta$ the compensating lithium ion is in fact bonded to one of the "shorter-bonded" oxygen atoms.

Some revealing observations come from comparison of "symmetrized" matrices $\mathbf{g}_{sym}$ and also $\mathbf{D}_{sym}$ (i.e., matrices averaged over the two (twofold) symmetry-related sites (configurations) 1 and 1′ of center $[FeO_4/Li]^0_\beta$, listed in Table II) with the corresponding matrices (Ref. 7, Table I) of the center $[FeO_4/Li]^0_\alpha$ (C_2 symmetry). Such averaging can occur in practice if the lithium jumps between symmetry-related locations. We note, first of all, that the sets of principal g values are virtually identical in the two cases. However, the corresponding principal directions perpendicular to axis $\hat{\mathbf{a}}_1$ are quite different; we note that the major difference comes from the respective azimuthal angles, which differ by 180°. The matrices $\mathbf{D}_{sym}$ of β and **D** of α show a striking similarity. We note (Table II) that the intermediate principal D values (roughly equal) correspond to axis $\hat{\mathbf{a}}_1$, while the respective principal directions of the two remaining values (differing roughly by a factor of 2 for centers α and β) are only 4° apart.

We tentatively suggest that forms α and β of the $[FeO_4/Li]^0$ center differ mainly in the location of the compensating lithium ion, the latter residing on one side of the "tetrahedron" in one form and on the opposite side in the other. At this time we do not yet fully understand the relationship between the observed spin-Hamiltonian parameter matrices and the structure of the Fe^{3+} center, but we can point out that similar effects were observed in the case of the two forms of lithium-compensated Ge^{3+} and Ti^{3+} centers in α-quartz, i.e., $[GeO_4/Li]^0_{A,C}$ (Ref. 2) and $[TiO_4/Li]^0_{A,B}$.[3,5] The most significant differences between the two forms of each of these centers, also considered to have the lithium ion on opposite sides of the "tetrahedron," are that the corresponding g values (with principal axes perpendicular to axis $\hat{\mathbf{a}}_1$) have interchanged principal axes.

B. $[FeO_4/H]^0_\beta$

We have accurately determined the spin-Hamiltonian parameters including matrices **g** and **D** and the hyperfine matrix $\mathbf{A}(^1H)$, as well as the Stevens parameters B_4^m for terms of type S^4 (Ref. 15) (Table III). No symmetry restrictions were imposed on the spin-Hamiltonian parameters during the fitting procedure, except that the hydrogen nuclear Zeeman matrix $\mathbf{g}_n(^1H)$ was kept isotropic with $g_n = 5.585\,691\,2$. The matrices **g** and **D** and the S^4 parameters were obtained from averaged EPR line positions (each taken as the center of gravity of the hydrogen hyperfine pattern). The final RMS deviation between 330 calculated and observed EPR line positions was 0.08 mT. To find the hyperfine matrix $\mathbf{A}(^1H)$, a total of 496 individual line positions taken from the (low-field) 3-4 and 5-6 transitions (see Figs. 5 and 7), showing clearly resolved ^1H hyperfine structure, were used. In the subsequent fitting procedure, only the $\mathbf{A}(^1H)$ matrix elements were varied; the final RMS deviation was 0.06 mT. Here we have chosen the sign of $\mathbf{A}(^1H)$ such that the unique principal value of the traceless part is positive, as expected for magnetic dipole-dipole interaction. With this choice, the sign of **D** is then not arbitrary.

The calculated EPR line positions of all symmetry-related $[FeO_4/H]^0_\beta$ centers (within the magnetic field range 0–1 T and for fixed microwave frequency 9915 MHz) for crystal rotation about axis $\hat{\mathbf{a}}_1$ (with $\hat{\mathbf{B}} \perp \hat{\mathbf{a}}_1$) are shown in Fig. 5. Thus, since here the crystal is rotated around a twofold symmetry axis, only three different symmetry-related spectra are observed; each transition is doubly degenerate in that plane.[20] The experimentally observed line positions are not shown in Fig. 5, since they fall on the curves at the scale used. Figure 7 shows an energy-level diagram as a function of **B**, for $\hat{\mathbf{B}} \| \hat{\mathbf{c}}$, indicating the EPR transitions occurring at 9915 MHz. A simulated c-axis spectrum (using the spin-Hamiltonian parameters in Table III) is presented in Fig. 8. It agrees well with the observed one.

TABLE II. $[FeO_4/Li]^0_\beta$ principal values and directions of matrices $\mathbf{Y} = \mathbf{g}$ and **D** averaged over sites 1 and 1′ (related by twofold symmetry axis $\hat{\mathbf{a}}_1$), in the crystal Cartesian coordinate system.

Y			k	Y_k	θ_k	φ_k
			$\mathbf{g}_{sym}$			
2.004 53	0	0	1	2.00 453	90	0
	2.003 84	−0.000 11	2	2.004 11	21.9	270
		2.004 07	3	2.003 80	111.9	270
			$\mathbf{D}_{sym}/h$ (MHz)			
−1193.3	0	0	1	3177.5	124.0	270
	1559.8	2394.4	2	−1193.3	90	0
		−366.5	3	−1984.2	34.0	270

TABLE III. Center $[FeO_4/H]^0_\beta$ principal values and directions of matrices $\mathbf{Y}=\mathbf{g}$, $\mathbf{D}$, and $\mathbf{A}(^1H)$ in the crystal Cartesian coordinate system[a] for site 1 at ca. 20 K, derived from EPR data. The S^4 parameter B_4^m are included as well.[15] The estimated uncertainties are appended, in parentheses.

Y			k	Y_k	θ_k	φ_k
		g				
2.004 31(12)	−0.000 41(9)	−0.000 38(7)	1	2.005 63(11)	121(2)	297(4)
	2.004 99(13)	0.000 66(7)	2	2.004 13(12)	78(17)	214(6)
		2.004 38(8)	3	2.003 91(8)	33(10)	322(19)
		D/h (MHz)				
−307.6(5)	4050.2(4)	1920.9(4)	1	4972.9(4)	47.357(3)	247.927(6)
	−1031.9(4)	−4389.8(4)	2	2235.1(3)	55.969(4)	16.382(5)
		1339.5(4)	3	−7208.0(4)	61.486(2)	127.905(3)
		$\mathbf{A}(^1H)/h$ (MHz)				
−4.1(1.5)	−7.7(4)	−2.6(8)	1	8.1(2)	68(2)	126(2)
	1.1(6)	2.5(4)	2	−2.0(7)	157(4)	114(14)
		−0.6(6)	3	−9.7(1.3)	86(6)	35(3)

B_4^m/h (MHz)

B_4^0/h	0.53(1)						
B_4^1/h	−1.22(5)	B_4^2/h	−1.05(3)	B_4^3/h	−7.11(12)	B_4^4/h	4.79(4)
B_4^{-1}/h	4.75(5)	B_4^{-2}/h	−0.29(2)	B_4^{-3}/h	1.58(13)	B_4^{-4}/h	0.65(5)

[a]Ref. 15, Table II: coordinate system (1).

Generally speaking, all the matrices constituting the spin Hamiltonian have principal values similar to those of the α-type hydrogen-compensated center.[10] The major differences between the corresponding matrices of α and β centers come from their different spatial orientations. The principal directions corresponding to the unique (negative) principal D value and the unique (positive) principal value of matrix $\mathbf{A}(^1H)$ are very close to the direction (Ref. 15, Table V) of the Si—O(2) bond in pure α-quartz, i.e., the shorter-type silicon-oxygen bond in the SiO_4 unit (see Ref. 1). The respective angles they make with Si—O(2) are only 5.6° and 3.0°, respectively. In the

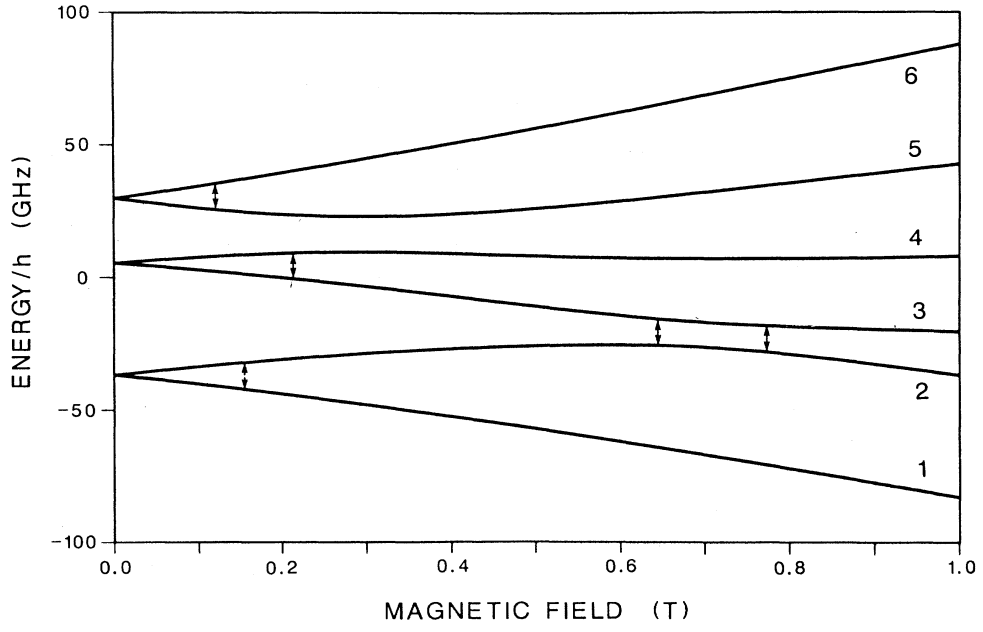

FIG. 7. The energy levels for $[FeO_4/H]^0_\beta$ as a function of external magnetic field ($\hat{\mathbf{B}}\|\hat{\mathbf{c}}$). No hyperfine splittings are included. Transitions at 9.915 GHz are indicated, and occur at (calculated) fields 120.33, 149.29, 212.12, 645.34, and 772.18 mT. The levels corresponding to the high-field m_s quantum numbers $-\frac{5}{2}$, $-\frac{3}{2}$ $-\frac{1}{2}$, $\frac{1}{2}$, $\frac{3}{2}$, and $\frac{5}{2}$ are numbered in order (of increasing energy) from 1 to 6.

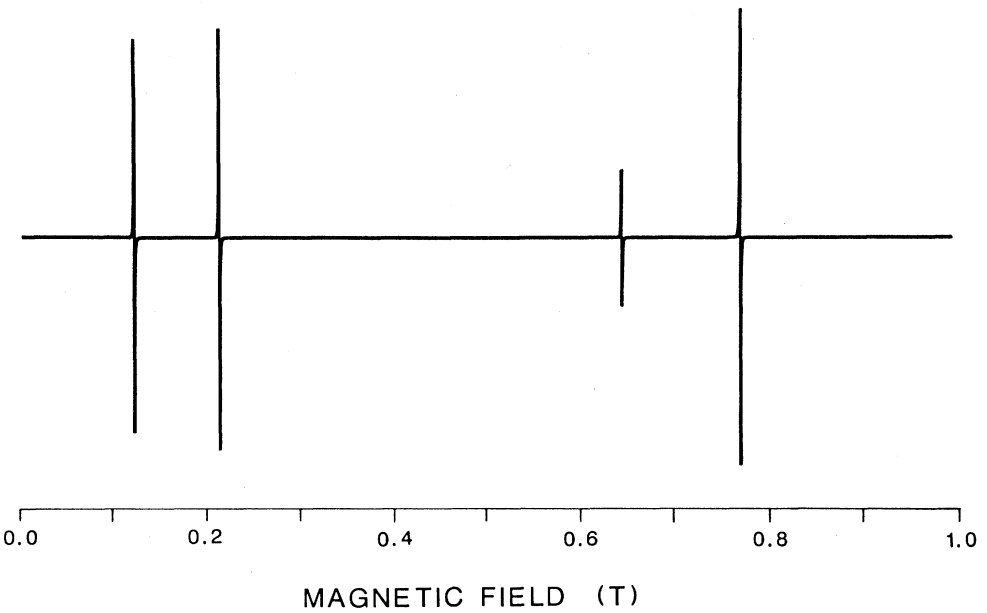

FIG. 8. First-derivative EPR spectrum of $[FeO_4/H]^0_\beta$ at 9.915 GHz simulated from the best-fit spin-Hamiltonian parameters in Table III, for $\hat{\mathbf{B}}\|\hat{\mathbf{c}}$ and excitation field $\hat{\mathbf{B}}_1\|\hat{\mathbf{a}}_1$. The transition at 149.29 mT (shown in Fig. 7) is not seen here due to its negligible intensity. The ^1H hyperfine splitting is not visible at the field scale used.

case of $[FeO_4/H]^0_\alpha$, the analogous principal directions are not far (1° and 31°, respectively) from the Si—O(4) (longer-type) bond. We conclude that the compensating H^+ ion in α and β type $[FeO_4/H]^0$ resides respectively at opposite sides of the $Si(Fe)O_4$ "tetrahedron," presumably in the c-axis channels. We note that the principal D values of the β center are somewhat smaller in magnitude than the corresponding ones of the α center, and that the matrix $\mathbf{D}$ of the former is closer to being uniaxial than that of the latter (as is true also for the Li pair). This can be expressed in terms of the D (uniaxial) and E (rhombic) parameters [defined as $D=3D_Z/(2h)$, $E=(D_Y-D_X)/(2h)$, where D_i $(i=X,Y,Z)$ are the principal values of matrix $\mathbf{D}$ obeying the condition $|D_Z|\geq|D_Y|\geq|D_X|$] and their ratio $|E/D|$ (ranging from 0 to $\frac{1}{3}$, for uniaxial and completely rhombic $\mathbf{D}$ matrix, respectively). For the $[FeO_4/H]^0_\beta$ center, $D=-10\,812.0(6)$ MHz, $E=1368.9(4)$ MHz, and $|E/D|=0.126\,61(4)$, whereas for $[FeO_4/H]^0_\alpha$, $D=-12\,179.9(8)$ MHz, $E=1747.8(6)$ MHz, and $|E/D|=0.143\,50(6)$. We note also that the center β has slightly more isotropic matrices $\mathbf{g}$ and $\mathbf{A}(^1H)$. In contrast to the center α, the isotropic part of $\mathbf{A}(^1H)$ of the center β has negative sign. We note that $\mathbf{A}(^1H)$ is further from being uniaxial in center β than in α, perhaps due to more appreciable spin density on one or more of the oxygen ions.

Since the geometric and electronic structures of these centers are not yet known in detail, we can at present only speculate as to whether these differences are related to the difference in the hydrogen-oxygen bond strength. It seems that the H^+ ion, due to its relatively large electron affinity and small size as compared to the alkali cations, can form a relatively strong bond with one oxygen atom (utilizing one of oxygen's lone electron pairs). That is probably the reason why both the α and β forms of the H-compensated Fe^{3+} center have the lowest (C_1) symmetry, at least up to room temperature, whereas the Li- and Na-compensated centers show changes to C_2 symmetry in this temperature range.

ACKNOWLEDGMENTS

The authors wish to thank L. E. Halliburton, J. J. Martin, A. S. Nowick, and B. Sawyer for making the samples available. This work was supported in part by the Natural Sciences and Engineering Research Council of Canada, and by the Department of Scientific and Industrial Research of New Zealand.

*On leave from Institute of Molecular Physics, Polish Academy of Sciences, Poznań, Poland.
†On leave from Chemistry Division, Department of Scientific and Industrial Research, Private Bag, Petone, New Zealand.

[1]J. A. Weil, Phys. Chem. Minerals **10**, 149 (1984).
[2]J. Isoya and J. A. Weil (unpublished). Also see Y. Haven, A. Kats, and J. S. van Wieringen, Philips Res. Rep. **21**, 446 (1966).
[3]M. Okada, H. Rinneberg, J. A. Weil, and P. M. Wright, Chem. Phys. Lett. **11**, 275 (1971).
[4]H. Rinneberg and J. A. Weil, J. Chem. Phys. **56**, 2019 (1972).
[5]J. Isoya, W. C. Tennant, and J. A. Weil, J. Magn. Reson. **79**, 90

(1988).
[6]R. H. D. Nuttall and J. A. Weil, Can. J. Phys. **59**, 1709 (1981).
[7]L. E. Halliburton, M. R. Hantehzadeh, J. Minge, M. J. Mombourquette, and J. A. Weil, Phys. Rev. B **40**, 2076 (1989).
[8]P. Stegger and G. Lehmann, Phys. Status Solidi B **151**, 463 (1989).
[9]J. Minge, M. J. Mombourquette, and J. A. Weil, Phys. Rev. B **40**, 6523 (1989).
[10]M. J. Mombourquette, J. Minge, M. R. Hantehzadeh, J. A. Weil, and L. E. Halliburton, Phys. Rev. B **39**, 4004 (1989).
[11]P. Stegger and G. Lehmann, Phys. Chem. Minerals **16**, 401 (1989).
[12]R. H. D. Nuttall and J. A. Weil, Can. J. Phys. **59**, 1696 (1981).
[13]R. H. D. Nuttall and J. A. Weil, Solid State Commun. **33**, 99 (1980).
[14]R. H. D. Nuttall and J. A. Weil, Can. J. Phys. **59**, 1886 (1981).
[15]M. J. Mombourquette, W. C. Tennant, and J. A. Weil, J. Chem. Phys. **85**, 68 (1986).
[16]M. J. Mombourquette, J. Minge, M. R. Hantehzadeh, J. A. Weil, and L. E. Halliburton (unpublished).
[17]J. Minge and J. A. Weil, J. Phys. Chem. Solids (to be published).
[18]D. Choi and S. H. Choh, J. Korean Phys. Soc. **21**, 107 (1988).
[19]B. D. Perlson and J. A. Weil, Rev. Sci. Instrum. **46**, 874 (1975).
[20]J. A. Weil, T. Buch, and J. E. Clapp, Adv. Magn. Reson. **6**, 183 (1973).